Superconducting Diode sensor

A. Sinner[1], X.-G. Wang[2], S. S. P. Parkin[3], A. Ernst[3,4], V. Dugaev[6], and L. Chotorlishvili[6]

[1]*Institute of Physics, University of Opole, 45-052 Opole, Poland*
[2] *School of Physics and Electronics, Central South University, Changsha 410083, China*
[3] *Max Planck Institute of Microstructure Physics, Weinberg 2, D-06120 Halle, Germany*
[4] *Institute for Theoretical Physics, Johannes Kepler University, Altenberger Straße 69, 4040 Linz, Austria*
[6] *Department of Physics and Medical Engineering,*
Rzeszów University of Technology, 35-959 Rzeszów, Poland
(Dated: June 21, 2023)

We study the superconducting Josephson junction diode operating via the magnetic field of skyrmions. Inspired by the near-field optical microscopy, we propose to partially screen the magnetic field and analyze part-by-part the magnetic texture of the skyrmion. The detected asymmetric supercurrent is influenced by the skyrmionic magnetic field and magnetic texture. This enables the Josephson junction diode to function as a hyperfine sensor and to read out the information about the morphology of the complex magnetic textures. The proposed setup opens a new avenue in magnetometry and represents an alternative to the technologies based on the nitrogen-vacancy centers.

Introduction: Diode is a device which exhibits the non-reciprocal responses and transport properties. The asymmetric conductance of the diode applies not only to the electric current but also its sonic counterparts, the propagation of acoustic vibrations, and the rectification of the heat transport at the nano-level. Recently the Josephson diode effect has been discovered [1–5]. In a Josephson junction, a thin metal or dielectric barrier layer separates two superconductors. When the inversion symmetry is broken by an external magnetic field, the Cooper pairs acquire a finite center-of-mass momentum, which leads to the phase mismatch between the left- and right-propagating currents and correspondingly to the asymmetric transport across the junction. This is the underlying mechanism of the Josephson diode effect.

In conventional Josephson junctions near the critical temperature, the current-phase relations are typically sinusoidal $j(\varphi) = j_c \sin(\varphi)$, where j_c is the critical current, $\varphi = \varphi_1 - \varphi_2$ is the difference between phases of the superconducting order parameters $\Delta_{1,2} = \Delta e^{i\varphi_{1,2}}$. In the systems with preserved time-reversal symmetry the current-phase relation is always antisymmetric $j(\varphi) = -j(-\varphi)$. By contrast, the broken time-reversal symmetry leads to the φ_0-type of the current-phase relations $j(\varphi) = j_c \sin(\varphi + \varphi_0)$, cf. [6, 7] for more details. The deeper analysis of the symmetry properties of the Onsager's coefficients suggests, that the two-terminal resistance must be even with respect to the magnetic field. This argument also applies to the case of the linear magnetoresistance, when resistance ϱ depends linearly on the magnetic field $\mathbf{B}$. Therefore to preserve the symmetry properties of the Onsager's coefficients, one needs to introduce an extra chiral term $\chi^{L/R}$ in the expression of the resistance $\varrho^{L,R}(\mathbf{k}, \mathbf{B}) = \varrho \left(1 + \chi^{L/R} \mathbf{I} \cdot \mathbf{B}\right)$ [8] for the left and right currents respectively. Here, $\mathbf{k}$ is the wave vector, I the current and the different sign $\chi^L = -\chi^R$ is required by the parity reversal symmetry. The occurrence of the chiral resistance $\varrho^{L,R}(\mathbf{k}, \mathbf{B})$ is the most essential consequence of the magnetochiral anisotropy. Recently, the experimental observation of the superconduct-
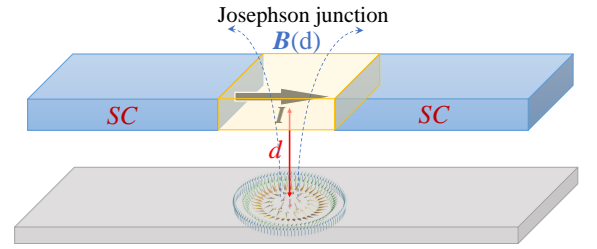

FIG. 1. The schematic representation of the Josephson junction sensing device. The magnetic field of the skyrmion breaks the inversion symmetry of the Josephson junction and gives rise to the superconducting diode effect. To increase the sensibility of the sensor, one can partially cover the skyrmion surface and analyse the effect of the magnetic field from the uncovered part. It is always possible to keep the open part of the skyrmion surface smaller than the characteristic size of the Josephson junction.

ing diode effect has been reported [1], which triggered a substantial theoretical interest in this phenomenon [2–5]. Although it has been known that the Josephson junction can sense small magnetic fields, only the effects of uniform constant external magnetic fields have been investigated that far.

The superconducting diode implies the effect of the nonreciprocal charge transport, which can be achieved when both, the spatial inversion and the time-reversal symmetries are broken. The Rashba spin-orbit term breaks the uniaxial spatial inversion symmetry along the $\mathbf{z}$-axis. The magnetochiral anisotropy is achieved in two realizations of external fields: (a) By applying the external magnetic field along the $\mathbf{y}$-axis and the electric field along the $\mathbf{x}$-axis. Then the non-reciprocal effect is quantified by the term $\varrho = \varrho_0 \left[1 + \gamma(\mathbf{B} \times \mathbf{z}) \cdot \mathbf{I}\right]$ [1]; (b) Alternatively one can direct electric field along the $\mathbf{z}$-axis. Then both, the magnetic field and the current are in-plane, leading to the chiral resistance term $\varrho = \varrho_0 \left[1 + \gamma(\mathbf{B} \times \mathbf{I}) \cdot \mathbf{z}\right]$ [5]. In previous studies, the

magnetic field in the expression of chiral resistance has been associated with some homogeneous external field [2–5]. In contrast to that, in the present project we will consider the magnetic field generated by the complex magnetic textures, such as for example the skyrmionic magnetic textures. In particular, the proximity effect of the skyrmion lattice or of individual skyrmions and stray magnetic fields can violate the $\mathcal{PT}$-symmetry. The skyrmion exerts the stray magnetic field (odd in $\mathcal{T}$ and even in $\mathcal{P}$) on the Josephson junction and violates $\mathcal{PT}$-symmetry. The superconducting diode should in principle feel the stray magnetic field and read out the information about the magnetic texture Fig.(1). In the present project, we propose the superfine superconducting diode sensor. Such a sensor can open new avenues in experimental skyrmionics, e.g. for studying the morphology of complex magnetic textures and systems. In particular, the superconducting diode sensors would be able to identify different magnetic phases, such as Néel and Bloch skyrmions, or ferromagnetic phases, and monitor transitions between them in a time domain.

In order to increase the sensibility of the superconducting Josephson junction sensor, we need to analyze the magnetic field (i.e., skyrmion magnetic texture) part by part separately for different flakes of the skyrmion texture. Thus we are looking for the spatially resolved effect. Near-field optical microscopy is a technology that allows covering the surface from unwanted electromagnetic interactions except for the small selected regions of 20-30nm in characteristic size. The magnetic field lines are closed loops. However, magnetic lines also can be redirected by offering them a preferred path (e.g., using high permeability materials to shield the magnetostatic field) [9]. Recent studies show that graphene can serve as a perfect shield due to its extraordinary properties [10].

The expression for the superconducting current can be derived phenomenologically [2, 4]. The free energy of the system has the form

$$F = -2|\gamma_1|\Delta^2\cos\varphi - |\gamma_2|\Delta^4\cos(2\varphi + \delta), \qquad (1)$$

where γ_1 and γ_2 denote the first- and second-order Cooper pair tunnelling processes. We derive the explicit expressions for $\gamma_{1,2}(\mathbf{B})$ from the microscopic theory. The key issue is the explicit dependence of coefficients $\gamma_{1,2}$ on the magnetic field. The phases in Eq. (1) are defined as follows: $\varphi = \varphi_2 - \varphi_1 + \arg(\gamma_1)$, $\delta = \arg(\gamma_2) - 2\arg(\gamma_1)$. The superconducting current $I(\varphi) = \frac{2\pi}{\Phi_0}\frac{\partial F}{\partial\varphi}$ becomes

$$I(\varphi) = \frac{2\pi}{\Phi_0}\left\{\Delta^2|\gamma_1|\sin\varphi + \Delta^4|\gamma_2|\sin(2\varphi + \delta)\right\}, \quad (2)$$

where $\Phi_0 = h/e$ denotes the superconducting flux quantum, e the charge of the electron. From Eq.(2) it is easy to see that the asymmetry between the left and right currents arises due to the term proportional to Δ^4. The skyrmions emerge in the thin magnetic films with broken inversion symmetry. The lack of inversion symmetry is associated with the Dzyaloshinskii–Moriya interaction

(DMI) [11–22]. Below we describe the magnetic texture of skyrmions by the local magnetization $\mathbf{M}(\mathbf{r})$. The dynamics of the local magnetization is governed by the phenomenological Landau-Lifshitz-Gilbert (LLG) equation

$$\frac{\partial\mathbf{M}}{\partial t} = -\gamma\mathbf{M}\times\mathbf{H}_{\text{eff}} + \frac{\alpha}{M_s}\mathbf{M}\times\frac{\partial\mathbf{M}}{\partial t}. \qquad (3)$$

Here, $\mathbf{M}(\mathbf{r}) = M_s\mathbf{m}$ describes the magnetic texture of the thin magnetic film, M_s being the saturation magnetization, $\mathbf{m}$ is the unit vector along the magnetization direction $\mathbf{M}$, and α is the phenomenological Gilbert damping constant. The total effective magnetic field $\mathbf{H}_{eff}$ reads $\mathbf{H}_{eff} = \frac{2A_{ex}}{\mu_0 M_s}\nabla^2\mathbf{m} + H_z\mathbf{z} - \frac{1}{\mu_0 M_s}\frac{\delta E_D}{\delta\mathbf{m}}$, where the first term describes the internal exchange field with the exchange stiffness A_{ex}, the second term corresponds to the external magnetic field H_z ($\mathbf{z}$ is a unit vector along the axis z normal to the film), while the last term is the DM field, with the DM interaction energy density $E_D = D_m[(m_z\frac{dm_x}{dx} - m_x\frac{dm_z}{dx}) + (m_z\frac{dm_y}{dy} - m_y\frac{dm_z}{dy})]$ and D_m being the strength of the DM interaction.

For numerical calculations we use the set of parameters which correspond to Co/heavy-metal multi-layers: $A_{ex} = 10\text{pJ/m}$, $D_m = 0.2\text{mJ/m}^2$, and $M_s = 1.2\times10^6\text{A/m}$. The bias magnetic field $H_z = 100$ mT is used for stabilization of the skyrmion structure. The skyrmion width is 45 nm. The size of the ferromagnetic layer is $3000\times240\times3\text{nm}^3$. The ferromagnetic layer is discretized with the cells of size $3\times3\times3\text{nm}^3$. Of particular importance is structure of the stray magnetic field $\mathbf{B}(\mathbf{m}(\mathbf{r}))$ generated by the magnetic skyrmion texture $\mathbf{m}(\mathbf{r})$. The explicit expression for the stray magnetic field can be derived analytically [23], but the derivation is rather involved and is placed into the Supplementary Information [24].

For the microscopic estimation of the parameters of the phenomenological free-energy Eq.(1) we exploit the Bogoliubov-deGennes Hamiltonian of the junction

$$\text{H}_{\text{BdG}} = \begin{pmatrix} h_0 - \mu & \boldsymbol{\Delta}_{0,1}^* & \boldsymbol{t}^* & 0 \\ \boldsymbol{\Delta}_{0,1} & -h_0 + \mu & 0 & \boldsymbol{t}^* \\ \boldsymbol{t} & 0 & h_0 - \mu & \boldsymbol{\Delta}_{0,2}^* \\ 0 & \boldsymbol{t} & \boldsymbol{\Delta}_{0,2} & -h_0 + \mu \end{pmatrix}, \quad (4)$$

where μ denotes the chemical potential, which is applied to both sides of the junction and $h_0 = -\frac{\hbar^2}{2m}\nabla^2$. $\boldsymbol{\Delta}_{0,i} = \Delta_0 e^{i\chi_i}$, $i = 1, 2$ denotes the mean-field order parameter in each superconductor of the junction. Furthermore, $\boldsymbol{t} = te^{i\xi}$ is the complex tunneling amplitude across the junction, related to the overlap of the electronic quantum wave functions on each superconducting side. Here we do not consider the tunneling matrix elements in the spin-flip channel, since flipping spins costs additional energy. To set up the free-energy energy functional, we have to consider the fluctuations in the order parameter above its mean-field value. In the simplest approximation, the

fluctuation term would read [25]

$$\delta \mathrm{H} = \begin{pmatrix} 0 & \mathbf{\Delta}_1^* & 0 & 0 \\ \mathbf{\Delta}_1 & 0 & 0 & 0 \\ 0 & 0 & 0 & \mathbf{\Delta}_2^* \\ 0 & 0 & \mathbf{\Delta}_2 & 0 \end{pmatrix}, \tag{5}$$

where $\mathbf{\Delta}_{1,2} = \Delta e^{i\varphi_{1,2}}$ are the time and position-dependent fluctuations of the order parameters corresponding to each superconductor. The free energy $\mathcal{F}$ is related to the grand-canonical partition function $\mathcal{Z}$ via

$$\mathcal{Z} = e^{-\mathcal{F}}, \tag{6}$$

where the properly normalized zero-temperature grand canonical partition function reads

$$\mathcal{Z}[\delta \mathrm{H}] = \lim_{\beta \to \infty} \frac{\mathrm{Tr}\ e^{-\beta(\mathrm{H}_{\mathrm{BdG}} + \delta \mathrm{H})}}{\mathrm{Tr}\ e^{-\beta \mathrm{H}_{\mathrm{BdG}}}}, \tag{7}$$

and $\beta = (k_B T)^{-1}$. Within the functional integrals formalism, the grand-canonical partition function Eq. (7) becomes

$$\mathcal{Z}[\delta \mathrm{H}] = \frac{1}{\mathcal{Z}_0} \int \mathcal{D}\bar{\Psi}\mathcal{D}\Psi\ e^{-\mathcal{S}[\bar{\Psi},\Psi]}, \tag{8}$$

where $\mathcal{Z}_0 = \mathcal{Z}[0]$. The corresponding action comprises two terms $\mathcal{S} = \mathcal{S}_{\mathrm{BdG}} + \delta\mathcal{S}$, where the first part corresponds to the mean-field Hamiltonian and the second to the term containing the fluctuations of the order parameters. Concretely we have $\mathcal{S}_{\mathrm{BdG}} = \bar{\Psi} \cdot [\hbar\partial_\tau \mathbb{1} + \mathrm{H}_{\mathrm{BdG}}]\Psi$, $\delta\mathcal{S} = \bar{\Psi} \cdot \delta \mathrm{H}\Psi$ with $\mathrm{H}_{\mathrm{BdG}}$ and $\delta \mathrm{H}$ defined in Eq. (4) and Eq. (5). The Grassmann fields $\psi^\dagger, \psi$, and $\varphi^\dagger, \varphi$ corresponding to both leads of the junction are combined to the Nambu bispinors $\bar{\Psi} = (\psi_\uparrow^\dagger, \psi_\downarrow, \varphi_\uparrow^\dagger, \varphi_\downarrow)$, where the up- and down-arrows denote two spin projections. The action is quadratic in Grassmann fields, and their integration can be performed exactly, which leads us to the general expression of the free energy as a function of fluctuations. The evaluation of this expression is conveniently performed by functional integrals, which leads us to

$$\mathcal{F}[\delta \mathrm{H}] = -\mathrm{tr}\log[\mathbb{1} + G_0\delta \mathrm{H}], \tag{9}$$

with the imaginary time Green's function

$$G_0(r\tau; r'\tau') = \langle r, \tau | [\partial_\tau \mathbb{1} + \mathrm{H}_{\mathrm{BdG}}]^{-1} | r'\tau' \rangle. \tag{10}$$

In the expansion in powers of $\delta \mathrm{H}$, we only keep terms which are present in the effective action Eq.(1). To the second order we get $\frac{1}{2}\mathrm{tr}(G_0\delta \mathrm{H})^2 \approx 2\gamma_1\Delta_1\Delta_2^* + 2\gamma_1^*\Delta_1^*\Delta_2 + \cdots$, with the coupling parameter

$$\gamma_1 \approx e^{-i(\chi_1 - \chi_2)} \frac{1}{2} \frac{\rho(E_F)t^2}{3!\Delta_0^2} \cos\gamma, \tag{11}$$

where $\gamma = 2\xi - \chi_1 + \chi_2$. The phases of the type γ often appear in multipartite superconducting systems, e.g. [26].

The density of states (DOS) for two spin projections of the 3d free electron gas at the Fermi surface reads

$$\rho_0(E_F) = \frac{1}{2\pi^2} \left(\frac{2m}{\hbar}\right)^{\frac{3}{2}} \frac{\sqrt{E_F}}{\Omega_{\mathrm{BZ}}}, \tag{12}$$

where Ω_{BZ} denotes the volume of the Brillouin zone. Hence, $\rho_0(E_F)$ and correspondingly γ_1 have the units of inverse energy. From the fourth order expansion term $\frac{1}{4}\mathrm{tr}(G_0\delta \mathrm{H})^4 \approx \gamma_2(\Delta_1\Delta_2^*)^2 + \gamma_2^*(\Delta_1^*\Delta_2)^2 + \cdots$ we extract the explicit form of the coupling parameter γ_2 as follows:

$$\gamma_2 \approx e^{-i(2\chi_1 - 2\chi_2 + \phi[\gamma])} \frac{\rho(E_F)t^2}{5!\Delta_0^4} g[\gamma], \tag{13}$$

which has the dimension of energy^{-3}. Here we have introduced $g[\gamma] = \sqrt{49\cos^2\gamma + 25\sin^2\gamma}$ and $\phi[\gamma] = \mathrm{atan}\left[\frac{5}{7}\tan\gamma\right]$. Note that in general, in Eqs. (11) and (13) the fluctuations depend on both time and spatial coordinates and the summation over these variables has to be understood. With Eq. (11) and (13) follows for the time-reversal symmetry breaking phase shift $\delta = \arg(\gamma_2) - 2\arg(\gamma_1) = \phi[\gamma]$. The diode current across the junction is proportional to $\sin[\delta]$, which gives $\delta I\left(\pm\frac{\pi}{2}\right) \sim \sin[\delta] \sim \sin[\gamma]$. Hence, the superconducting diode effect is rather general and in principle should be observable in any junction even without an external magnetic field. However, it is to expect that without an external field, the angle γ is very small and the diode current would be suppressed by the thermal or mechanical noise. In the presence of the magnetic field, the phase difference is fixed to $\delta = 2\frac{e}{\hbar}\oint_\mathcal{C} d\mathbf{r} \cdot \mathbf{A}$ with the vector potential $\mathbf{A}$ related to the magnetic field via $\mathbf{B} = \mathbf{curl A}$ and factor 2 counting two superconductors on both sides of the junction [24]. Finally we use the Stokes theorem $\oint_\mathcal{C} d\mathbf{r} \cdot \mathbf{A} = \int_S d\mathbf{S} \cdot \mathbf{curl A} = \int_S d\mathbf{S} \cdot \mathbf{B}$. For instance this yields for the homogeneous y-directed magnetic field [24]

$$\delta = 2B_y \frac{e}{\hbar} \int_0^h dz \int_0^{\lambda_L} dx = \frac{B_y}{B_d}, \tag{14}$$

where h is the height of the superconducting lead and λ_L the London penetration length. Introducing the flux Φ we can further write $\delta = h\lambda_L \frac{e}{\hbar} B_y = 2\pi \frac{\Phi}{\Phi_0}$. Eq. (14) recovers the earlier result of the work [4].

The magnetic stray field $\mathbf{B}(\mathbf{r})$ induced by the skyrmion does not only influence the phases of the condensate but also the coupling parameters of the free energy, entering it via the density of the states. The complexity of our problem is due to the fact that the magnetic stray field is not uniform, and the corresponding Hamiltonian $\hat{h}(\mathbf{B}) = -\frac{\hbar^2}{2m}\nabla_r^2\sigma_0 + \mu_B\boldsymbol{\sigma} \cdot \mathbf{B}(\mathbf{r})$, with $\mu_B = e\hbar/(2m) \approx 5.63 \cdot 10^{-5}\mathrm{eV/T}$ being the Bohr's magneton and the Lande factor assumed to be 2, cannot be generally diagonalized exactly. Thus the problem in our case is much more demanding than in earlier studies. The cumbersome evaluation and the final results for the DOS are presented in the Supplementary Information [24].
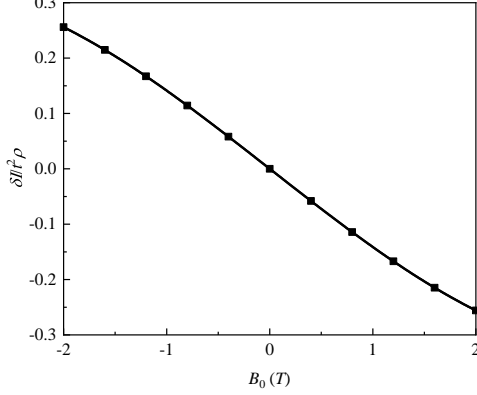
FIG. 2. The dependence of the supercurrent asymmetry $\frac{\delta I}{t^2 \rho(E_F, B)}$ on homogeneous external magnetic field. Varying the external magnetic field from $B_0 < 0$ to $B_0 > 0$ we observe the change of the sign of current asymmetry

The effect of the magnetic field on the DOS arises from both, the topography (i.e. Néel or Bloch skyrmion) and the geometry (size) of the magnetic texture. Our aim is to explore these parameters via the rectification of the superconducting diode current. The details of calculations are presented in the Supplementary Information [24]. The resulting supercurrent asymmetry reads

$$\delta I = -t^2 \rho(E_F, \mathbf{B}) \frac{|\Delta|^4}{3\Delta_0^4} \sin[\delta]. \qquad (15)$$

We calculate the phase difference $\delta = \chi_2 - \chi_1$ with the Stokes' theorem $\oint_{\mathcal{C}} d\mathbf{r} \cdot \mathbf{A} = \int_S d\mathbf{S} \cdot \mathbf{B}$. Taking account of the particular device geometry we acquire:

$$\delta = \frac{4\pi}{\phi_0} \int\limits_0^{\lambda_L} dx \int\limits_{-\frac{W}{2}}^{\frac{W}{2}} dy \; B_z, \qquad (16)$$

where λ_L is the London penetration length. The explicit form of the skyrmion field B_z is given in [24].

Discussions: The skyrmion magnetic field enters the supercurrent asymmetry Eq. (15) via the DOS and the phase factor. First we study the dependence of the supercurrent asymmetry $\frac{\delta I}{t^2 \rho(E_F, \mathbf{B})}$ on the external homogeneous magnetic field. Varying the values of the external magnetic field from negative $B_0 < 0$ to positive $B_0 > 0$ value, we observe the change of the sign of current asymmetry shown in the left panel of Fig. 2. A similar behavior is expected to be seen in the case of the inhomogeneous field of a skyrmion. To increase the sensitivity of the diode sensor, we screen most of the surface of the skyrmion and leave the small flake region uncovered to contribute to the effect. The center of the unscreened square region with the size 6×6 nm is spatially separated from the skyrmion center at $(x = 0, y = 0)$ by a
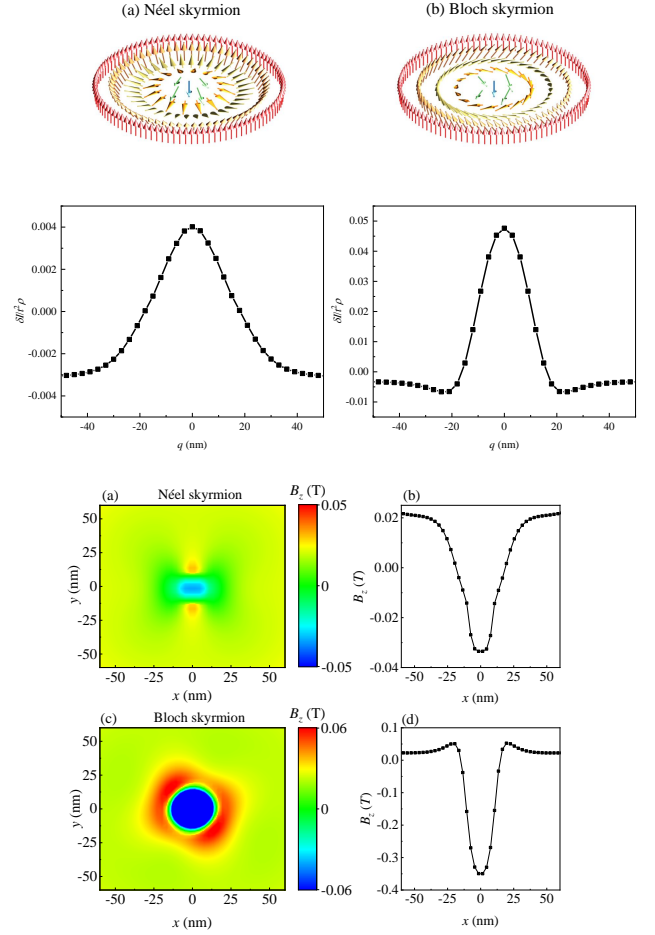

FIG. 3. **Top:** Variation of the supercurrent asymmetry in an inhomogeneous skyrmion field for (a) Néel and (b) Bloch skyrmions. q is the distance from the unscreened region to the center of the skyrmion at $(x = 0, y = 0)$. **Bottom:** Skyrmion magnetic field component $B_z(x, y)$ as function of the distance from the skyrmion center $(x = 0, y = 0)$. (b), (d) Crosssection profiles of the magnetic field components $B_z(x, y = 0)$ for (b) Néel and (d) Bloch skyrmions. The distance between the skyrmion and the diode is $d = 1.5$nm for all figures.

characteristic distance q. It makes the superconducting diode a hyperfine spatially resolved sensor. The amplitude and the spatially resolved profile of the asymmetry rectification effect depend on the type of skyrmion and magnetic texture. This is shown in the upper panel in Fig. 3. Changing of the sign of δI we can vary the sign of the corresponding spatially resolved magnetic field and the magnetic texture, cf. the bottom panel of Fig. 3.

Summary: In this paper we develop the phenomenological and theoretical framework of the hyperfine sensing device based on the superconducting Josephson diode effect. The main purpose of the device is to investigate the structure of the magnetic films textures with special emphasis on the high precision skyrmion morphology and location detection. By screening off large areas of the films, e.g. by graphene microshields, the effective exit area of

the magnetic field is reduced to the scales comparable to the typical size of the Josephson junction. The sensing process consists in tracking the supercurrent anysotropy, which is influenced by the magnetic field of the film. Our theoretical modelling demonstrates persuasively that the supercurrent anysotropy imitates the topography of the investigated magnetic tissue of the film.

[1] F. Ando, Y. Miyasaka, T. Li, J. Ishizuka, T. Arakawa, Y. Shiota, T. Moriyama, Y. Yanase, and T. Ono, Nature **584**, 373 (2020).

[2] K.-R. Jeon, J.-K. Kim, J. Yoon, J.-C. Jeon, H. Han, A. Cottet, T. Kontos, and S. S. Parkin, Nature Materials **21**, 1008 (2022).

[3] B. Pal, A. Chakraborty, P. K. Sivakumar, M. Davydova, A. K. Gopi, A. K. Pandeya, J. A. Krieger, Y. Zhang, S. Ju, N. Yuan, *et al.*, Nature physics **18**, 1228 (2022).

[4] M. Davydova, S. Prembabu, and L. Fu, Science advances **8**, eabo0309 (2022).

[5] C. Baumgartner, L. Fuchs, A. Costa, S. Reinhardt, S. Gronin, G. C. Gardner, T. Lindemann, M. J. Manfra, P. E. Faria Junior, D. Kochan, *et al.*, Nature Nanotechnology **17**, 39 (2022).

[6] A. Buzdin, Phys. Rev. Lett. **101**, 107005 (2008).

[7] A. Daido, Y. Ikeda, and Y. Yanase, Phys. Rev. Lett. **128**, 037001 (2022).

[8] G. L. J. A. Rikken, J. Fölling, and P. Wyder, Phys. Rev. Lett. **87**, 236602 (2001).

[9] S. Grabchikov, A. Trukhanov, S. Trukhanov, I. Kazakevich, A. Solobay, V. Erofeenko, N. Vasilenkov, O. Volkova, and A. Shakin, Journal of Magnetism and Magnetic Materials **398**, 49 (2016).

[10] Y. Chen, J. Li, T. Li, L. Zhang, and F. Meng, Carbon **180**, 163 (2021).

[11] J. White, K. Prša, P. Huang, A. Omrani, I. Živković, M. Bartkowiak, H. Berger, A. Magrez, J. Gavilano, G. Nagy, *et al.*, Phys. Rev. Lett. **113**, 107203 (2014).

[12] A. Derras-Chouk, E. M. Chudnovsky, and D. A. Garanin, Phys. Rev. B **98**, 024423 (2018).

[13] S. Haldar, S. von Malottki, S. Meyer, P. F. Bessarab, and S. Heinze, Phys. Rev. B **98**, 060413 (2018).

[14] C. Psaroudaki, S. Hoffman, J. Klinovaja, and D. Loss, Phys. Rev. X **7**, 041045 (2017).

[15] K. A. van Hoogdalem, Y. Tserkovnyak, and D. Loss, Phys. Rev. B **87**, 024402 (2013).

[16] S. Rohart, J. Miltat, and A. Thiaville, Phys. Rev. B **93**, 214412 (2016).

[17] S. Tsesses, E. Ostrovsky, K. Cohen, B. Gjonaj, N. Lindner, and G. Bartal, Science **361**, 993 (2018).

[18] X.-g. Wang, L. Chotorlishvili, G.-h. Guo, and J. Berakdar, J. Appl. Phys. **124**, 073903 (2018).

[19] X.-g. Wang, L. Chotorlishvili, G.-h. Guo, C.-L. Jia, and J. Berakdar, Phys. Rev. B **99**, 064426 (2019).

[20] X.-G. Wang, L. Chotorlishvili, G. Tatara, A. Dyrdał, G.-h. Guo, V. K. Dugaev, J. Barnaś, S. Parkin, and A. Ernst, Phys. Rev. B **106**, 104424 (2022).

[21] X.-g. Wang, G.-h. Guo, V. K. Dugaev, J. Barnaś, J. Berakdar, S. S. P. Parkin, A. Ernst, and L. Chotorlishvili, Phys. Rev. B **107**, 094404 (2023).

[22] V. Vijayan, L. Chotorlishvili, A. Ernst, S. S. P. Parkin, M. I. Katsnelson, and S. K. Mishra, Phys. Rev. B **107**, L100419 (2023).

[23] Y. Dovzhenko, F. Casola, S. Schlotter, T. Zhou, F. Büttner, R. Walsworth, G. Beach, and A. Yacoby, Nature communications **9**, 1 (2018).

[24] Supplementary Material.

[25] A. Sinner, Y. E. Lozovik, and K. Ziegler, Phys. Rev. Research **2**, 033085 (2020).

[26] A. Sinner, Y. E. Lozovik, and K. Ziegler, Phys. Rev. B **104**, 245124 (2021).